Applied Physics Letters

RESEARCH ARTICLE | MARCH 20 2026

Wavelike thermal phonons revealed by localization in graphene phononic crystals

Special Collection: Thermal Properties of Graphene and Carbon Materials – From Physics to Applications in Thermal Management

Bin Liu ; Zhiguo Tian ; Alexander A. Barinov ; Moran Wang

Appl. Phys. Lett. 128, 112206 (2026)
https://doi.org/10.1063/5.0316529

Applied Physics Letters ARTICLE pubs.aip.org/aip/apl

Wavelike thermal phonons revealed by localization in graphene phononic crystals

Cite as: Appl. Phys. Lett. **128**, 112206 (2026); doi: 10.1063/5.0316529
Submitted: 13 December 2025 · Accepted: 5 March 2026 ·
Published Online: 20 March 2026

Bin Liu,[1] Zhiguo Tian,[1] Alexander A. Barinov,[2] and Moran Wang[1,a)]

AFFILIATIONS

[1]Key Laboratory for Thermal Science and Power Engineering of Ministry of Education, Department of Engineering Mechanics, Tsinghua University, Beijing 100084, China
[2]Department of Thermophysics, Bauman Moscow State Technical University, Moscow 105005, Russia

Note: This paper is part of the Special Topic, Thermal Properties of Graphene and Carbon Materials — From Physics to Applications in Thermal Management.
[a)]**Author to whom correspondence should be addressed:** mrwang@tsinghua.edu.cn

ABSTRACT

The high Debye temperature and ultralong phonon mean free paths (MFPs) of graphene phononic crystals (GPnCs) enable wavelike phonon transport to manifest over extended length scales, making them an ideal platform for studying phonon localization. We employ machine-learning molecular dynamics to investigate thermal transport in periodic and aperiodic GPnCs. By combining homogeneous non-equilibrium molecular dynamics and non-equilibrium molecular dynamics, we directly extract the spectrally decomposed phonon MFP applicable to aperiodic structures. Spectral analysis establishes characteristic frequency ($\omega_c \approx 10$ THz) and length ($L_c \approx 100$ nm) scales for localization effects, and the nonlinear deviation in the $1/\kappa$–$1/L$ relationship (κ: thermal conductivity) indicates the presence of localized phonons. Lattice dynamics reveals that the increased fraction of low-participation-ratio modes and the absence of high-group-velocity modes in aperiodic graphene phononic crystals (ap-GPnC) uncover the microscopic origin of disorder-induced phonon localization. Elastic wave simulations further provide direct wave-field evidence of pronounced spatial localization of low-frequency phonons in ap-GPnC with increasing propagation distance.

Precise control of nanoscale thermal transport is a challenge in thermoelectric energy conversion and microelectronic thermal management.[1] Conventional phonon scattering strategies, including alloying, nanoparticle embedding, and interface engineering, primarily reduce phonon mean free paths (MFPs) by introducing incoherent scattering centers, with physical limits from saturation when the phonon MFP becomes comparable to the lattice constant.[2–6] Anderson localization of wavelike (coherent) phonons offers a new pathway to transcend this limit: in disordered systems, when the spatial distribution of scattering centers breaks the long-range translational symmetry of the structure, phonon wave functions may become exponentially localized in space, leading to strong suppression of thermal transport.[7–11]

Although Anderson localization offers theoretical promise for thermal conductivity reduction, its experimental and computational identification remains challenging. Thermal transport simultaneously involves two channels: coherent phonons (maintaining phase relationships) and incoherent phonons.[12,13] When structural disorder is introduced, coherent phonons may undergo Anderson localization with their thermal conductance contribution decaying exponentially;[14] however, incoherent phonons are insensitive to disorder and continue to follow ballistic-diffusive transport laws.

The intrinsic mode-dependence of phonon coherence necessitates mode-level analysis for reliable localization identification, since the length dependence of total thermal conductivity alone is insufficient. However, a theoretical framework for decoupling coherent and incoherent thermal transport at this level is still lacking.[15,16] Microscopic information, such as spectrally decomposed phonon MFPs, group velocity distributions, and wave field propagation characteristics, can provide physical insights inaccessible to macroscopic measurements, which is crucial for distinguishing the transport behaviors of different phonon modes and identifying localization effects.[17–21]

Molecular dynamics simulation is a powerful tool for investigating phonon transport in nanostructures. Interatomic potentials inherently contain anharmonic terms of all orders, enabling simultaneous capture of both coherent and incoherent phonon transport.[13] The development of machine-learning potentials has achieved a balance between near first-principles accuracy and high computational

efficiency, making it possible to construct large-scale complex nanostructures.[22–26]

Graphene phononic crystals (GPnCs) represent an ideal platform for studying wavelike phonon localization.[27,28] Graphene possesses an exceptionally high Debye temperature (~2000 K) and ultralong phonon MFPs (reaching hundreds of nanometers to micrometers at room temperature),[29–31] allowing coherent phonons to propagate sufficiently long distances before phase destruction by intrinsic scattering.

In this work, we employ machine-learning molecular dynamics simulations based on the neuroevolution potential (NEP) to systematically investigate the thermal transport properties of periodic graphene phononic crystals (p-GPnC) and aperiodic graphene phononic crystals (ap-GPnC).[26,32,33] The interatomic interactions are described by the general-purpose carbon NEP developed by Fan *et al.*, which has been successfully applied to thermal transport studies of graphene nanostructures.[29,34,35] Figure 1(a) illustrates the schematic of the nonequilibrium molecular dynamics (NEMD) simulation setup. Both p-GPnC and ap-GPnC are constructed from graphene nanoribbons by removing selected carbon atoms to form nanopores. The two structures maintain identical porosity and average pore spacing: nanopores in p-GPnC are arranged in a strictly periodic pattern, whereas in ap-GPnC, the nanopore position within each unit cell is randomly selected from predefined candidate sites. The spectral thermal conductance is calculated using the spectral heat current method implemented in the GPUMD package, and all thermal conductance G and thermal conductivity κ results are quantum-corrected (supplementary material, Secs. S1–S3).[17,26,36–38]

This system has been previously studied using a two-phonon model to separate coherent and incoherent phonon contributions,[15,39,40] providing reference benchmarks. As shown in Fig. 1, our calculated thermal conductivity of p-GPnC increases monotonically with length, following the standard ballistic-to-diffusive transition. In contrast, the thermal conductivity increase in ap-GPnC is significantly suppressed at short lengths. Two-phonon model fitting (supplementary material, Sec. S4) reveals that the coherent phonon contribution in ap-GPnC exhibits non-monotonic length dependence, reaching a maximum at approximately 16 nm before declining, which is a characteristic signature of Anderson localization. The fitted localization length (approximately 24 nm) is comparable to the previously reported value of 33 nm,[39] validating the reliability of the machine-learning potential and simulation methodology employed here.

The central objective of this work is to elucidate the microscopic mechanisms of Anderson localization at the mode level. We extract spectrally decomposed phonon MFPs by combining homogeneous non-equilibrium molecular dynamics (HNEMD) and NEMD.[26,41] This approach does not rely on Brillouin zone definitions and is applicable to aperiodic structures lacking translational symmetry. We further integrate lattice dynamics calculations and elastic wave propagation simulations to establish a multi-level analysis framework for identifying wavelike phonon localization.

The evolution of $\Delta G(\omega, L) = G_p - G_{ap}$ [Fig. 2(a)] demonstrates that the thermal transport difference between p-GPnC and ap-GPnC is concentrated in the low-frequency region ($\omega < 10$ THz) and at short lengths ($L < 100$ nm). This dual selectivity in frequency and length directly reflects the sensitivity of coherent phonons to structural disorder. Low-frequency phonons possess longer coherence lengths and are therefore more sensitive to the disruption of periodic structure. As length increases, the contribution of localized coherent phonons

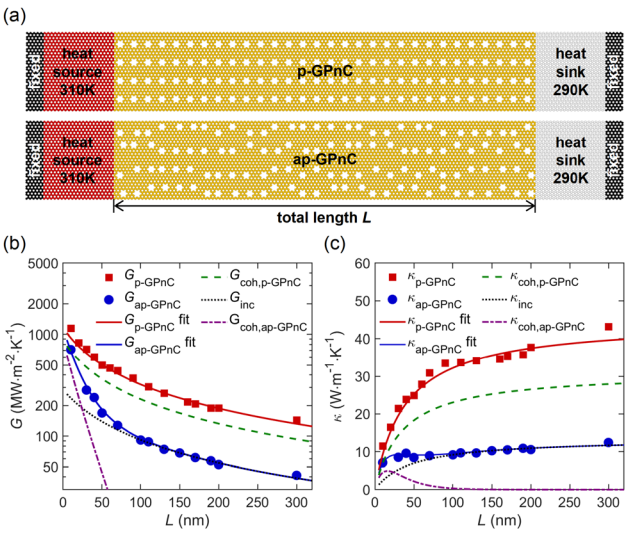

FIG. 1. (a) NEMD simulation setup for p-GPnC and ap-GPnC. (b) Thermal conductance G vs total length L. Red squares and blue circles: simulation data for p-GPnC and ap-GPnC, respectively; solid lines: two-phonon model fits; green dashed and purple dash-dotted lines: coherent contributions; black dotted line: incoherent contribution. (c) Thermal conductivity κ vs L.

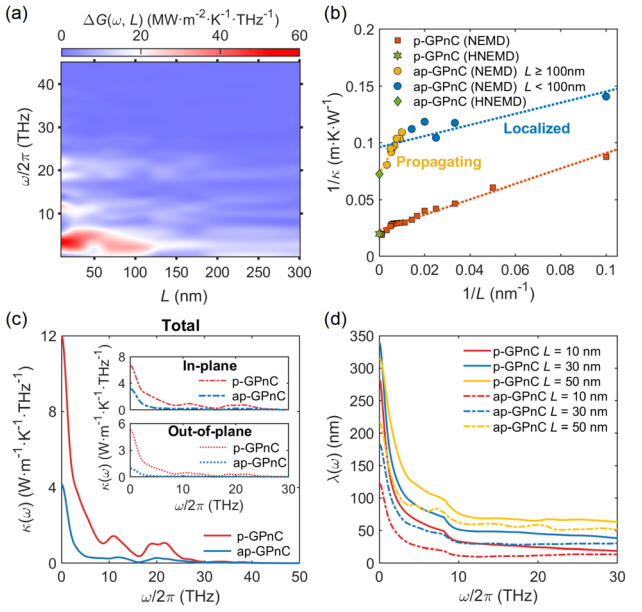

FIG. 2. Spectral thermal transport analysis. (a) Evolution of the spectral thermal conductance difference $\Delta G(\omega, L) = G_p - G_{ap}$ between p-GPnC and ap-GPnC vs frequency and total length. (b) Schelling plot ($1/\kappa$ vs $1/L$). p-GPnC (red squares) exhibits good linearity; ap-GPnC data are distinguished by $L < 100$ nm (blue circles) and $L \geq 100$ nm (orange circles). Green dots denote HNEMD reference values. (c) HNEMD spectral thermal conductivity $\kappa(\omega)$ at 300 K ($L = 500$ nm). Insets show in-plane and out-of-plane contributions. (d) Spectrally decomposed phonon MFP $\lambda(\omega)$ at different lengths.

decays exponentially, and the difference between the two structures converges. The critical frequency and length serve as characteristic parameters for distinguishing coherent-dominated and incoherent-dominated transport regimes.[13,42]

In Fig. 2(b), we employ the finite-size extrapolation (Schelling extrapolation) based on the Landauer framework to analyze the length dependence of thermal conductivity. Within the standard ballistic-diffusive transport framework, $1/\kappa$ and $1/L$ should exhibit a linear relationship: $1/\kappa = 1/\kappa_{\text{bulk}} + \lambda/(\kappa_{\text{bulk}} \cdot L)$. The p-GPnC data exhibit good linearity over the entire length range, and the extrapolated bulk thermal conductivity agrees well with the HNEMD reference value (supplementary material, Sec. S5), indicating that thermal transport is dominated by propagating phonons. In contrast, the full-data fit for ap-GPnC deviates significantly from linearity, with the extrapolated thermal conductivity (blue dashed line) underestimating the HNEMD reference by approximately 24.6%. This deviation is a characteristic signature of Anderson localization, where the exponential decay of localized coherent phonons causes the $1/\kappa$–$1/L$ relationship to curve upward in the short-length regime. When the fit is restricted to $L \geq 100$ nm (orange circles), linearity is significantly restored, and the extrapolated value deviates from the HNEMD reference by only 0.5%. According to the two-phonon model, at $L = 100$ nm, $\exp(-L/L_{\text{loc}}) = \exp(-100/24) \approx 0.015$, indicating that the localized coherent phonon contribution has decayed to a negligible level. Therefore, the degree of nonlinear deviation in the $1/\kappa$–$1/L$ relationship can serve as a diagnostic criterion for the presence of localized phonon modes.

Figure 2(c) shows that the total spectral thermal conductivity of ap-GPnC is significantly lower than that of p-GPnC in the low-frequency region, while the two converge in the high-frequency region. The insets further decompose the thermal conductivity into in-plane (longitudinal/transverse acoustic, LA/TA modes) and out-of-plane (flexural acoustic, ZA modes) contributions. The in-plane/out-of-plane decomposition analysis (supplementary material, Fig. S7) reveals that the relative contribution of out-of-plane modes in p-GPnC exhibits strong temperature dependence, varying from approximately 11% at 100 K to approximately 38% at 300 K, whereas this temperature dependence is significantly compressed in ap-GPnC (20%–27%). This phenomenon indicates that the scattering mechanisms introduced by structural disorder compete with temperature-dependent intrinsic phonon scattering, thereby altering the relative contributions of different polarization branches to thermal transport.

Figure 2(d) presents the spectrally decomposed phonon MFP extracted using $\lambda(\omega) = \kappa(\omega)/G(\omega)$, which combines the intrinsic spectral thermal conductivity $\kappa(\omega)$ obtained from HNEMD with the finite-length spectral thermal conductance $G(\omega)$ obtained from NEMD. The results reveal that the spectral MFP of ap-GPnC is lower than p-GPnC, with a faster decay rate and earlier convergence to a lower asymptotic value. The difference in $\lambda(\omega)$ between the two structures is concentrated primarily in the low-frequency region ($\omega < 10$ THz), corroborating the conclusions from Figs. 2(a) and 2(c). Notably, in the very low-frequency region, the initial values of $\lambda(\omega)$ for p-GPnC at different lengths are relatively close to each other, whereas ap-GPnC exhibits pronounced length dependence. This behavior is a direct manifestation of localization effects, as the exponential decay of localized coherent phonons significantly reduces the effective MFP in the short-length regime.

To understand the microscopic origins of thermal transport differences between the two structures, we calculate the phonon properties of p-GPnC and ap-GPnC using machine-learning potentials combined with lattice dynamics methods (Fig. 3). The force constant matrix is computed using the finite displacement method via the calorine package,[43] followed by diagonalization of the dynamical matrix using phonopy (supplementary material, Sec. S6).[44] We focus on the low-frequency region (0–10 THz), where phonon branches remain relatively well-defined and where, according to Fig. 2(a), the spectral thermal conductance differences induced by phonon localization are primarily located.

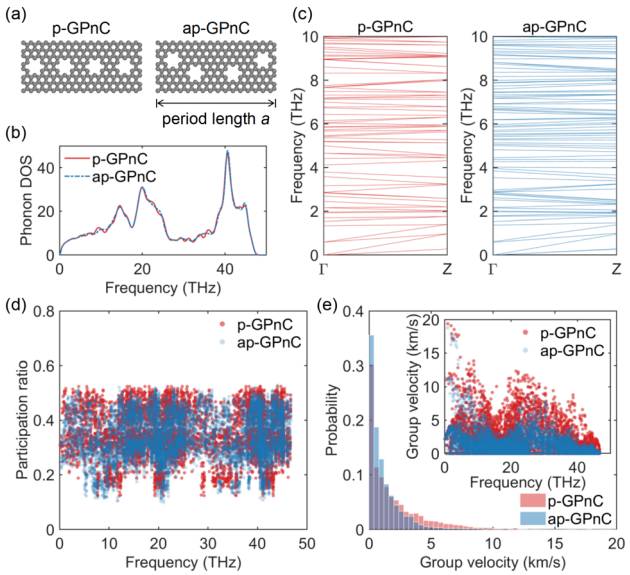

FIG. 3. Comparison of phonon properties between p-GPnC and ap-GPnC with unit cell length $a = 4$ nm. (a) Schematic of the unit cell structure; (b) phonon density of states (DOS); (c) low-frequency (0–10 THz) phonon dispersion along the thermal transport direction $\Gamma \rightarrow Z$; (d) phonon participation ratio distribution; (e) group velocity probability distribution, with the inset showing group velocity as a function of frequency. Phonon properties over the full frequency range for different unit cell lengths ($a = 1$, 2 nm) are provided in supplementary material Figs. S9–S13.

At the current computational scale, the phonon density of states (DOS) of the two structures nearly overlaps [Fig. 3(b)], indicating that structural disorder over finite length scales does not significantly alter the total number of phonon modes or their frequency distribution. Therefore, the origin of thermal conductivity differences should be sought in mode-level transport properties, such as group velocity and participation ratio. The phonon dispersion relations in Fig. 3(c) reveal the essential distinction between the two structures. p-GPnC exhibits clear band structure with well-defined dispersion slopes along the $\Gamma \rightarrow Z$ direction. In contrast, the bands of ap-GPnC become flattened, especially in the low-frequency region ($\omega < 10$ THz), corresponding to reduced group velocities.[28,45,46]

Figure 3(d) shows that the phonon participation ratios of both structures are predominantly concentrated in the range of 0.2–0.6, indicating that most phonon modes are neither fully localized nor fully extended. As shown in supplementary material Figs. S11 and S12, with increasing period length, the differences in participation ratio distributions between the two structures become more apparent: at $a = 4$ nm and $a = 6$ nm, the participation ratio distribution of ap-GPnC shifts noticeably toward lower values compared to p-GPnC. These

eigenmode-level characteristics are consistent with the thermal transport differences observed in molecular dynamics simulations.

The group velocity distribution in Fig. 3(e) further corroborates the above analysis. The overall group velocity of ap-GPnC is significantly lower than that of p-GPnC, with the probability distribution clearly shifted toward lower velocities. p-GPnC possesses numerous high group velocity modes (5–15 km/s), whereas these high-velocity modes are largely absent in ap-GPnC. Group velocity is a key parameter determining phonon thermal transport capability, and its systematic reduction directly leads to a significant decrease in thermal conductivity of ap-GPnC.

The length scale of lattice dynamics calculations ($a = 4$ nm, quasi-random) is much smaller than the system lengths in molecular dynamics simulations. For ap-GPnC, as system size increases, the cumulative effects of disorder may lead to more pronounced localization. However, Fig. 2(a) shows that spectral thermal conductance differences between the two structures are concentrated primarily in the $L \leq 100$ nm range and are more pronounced at smaller L. Therefore, the band flattening and group velocity reduction mechanisms revealed by small-scale lattice dynamics calculations can provide microscopic explanations for the thermal transport behavior observed in molecular dynamics simulations.

To visualize the propagation and localization behavior of wave-like phonons, we employ the finite element method (FEM) to solve the frequency-domain wave equation and simulate the scattering of plane longitudinal waves in p-GPnC and ap-GPnC (Fig. 4). These simulations provide complementary perspectives on frequency-dependent wave propagation characteristics.

The two structures exhibit different propagation characteristics at low frequency (5 THz). In p-GPnC, elastic waves effectively penetrate the entire structure, with the acoustic pressure field displaying regular interference fringes that reflect coherent Bloch wave propagation in the periodic structure. In contrast, ap-GPnC exhibits pronounced wave localization. As propagation distance increases, wave amplitude becomes significantly enhanced in local regions forming "hotspots," while overall transmitted energy is substantially attenuated. This behavior becomes more pronounced with increasing system length, consistent with the Anderson localization theory.

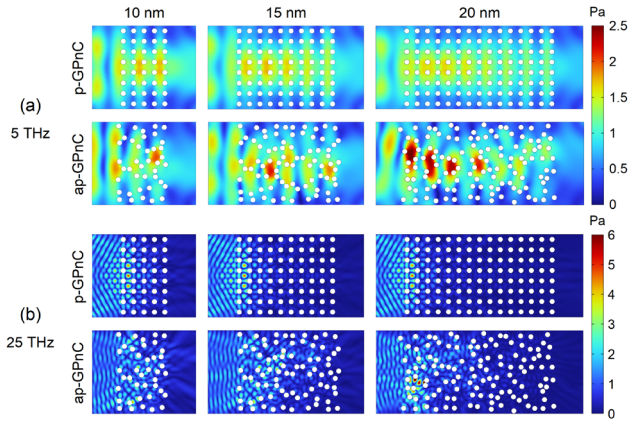

FIG. 4. Scattered field distributions of elastic waves in p-GPnC and ap-GPnC at (a) 5 THz and (b) 25 THz for total length $L = 10$, 15, and 20 nm. The color scale indicates the acoustic pressure amplitude. Plane longitudinal waves are incident from the left boundary, and nanopores are represented by white circles.

At intermediate frequency (25 THz), the difference in scattered field distributions between the two structures diminishes significantly. Both p-GPnC and ap-GPnC exhibit relatively uniform wave field distributions, with no pronounced localization phenomena observed. Results at 45 THz (supplementary material, Fig. S14) are similar, further indicating that intermediate- and high-frequency elastic waves are insensitive to structural periodicity. This is consistent with the analyses in Figs. 2 and 3, where high-frequency phonons enter the diffusive transport-dominated regime due to enhanced intrinsic scattering and shortened coherence lengths, and structural disorder has limited influence.

The FEM simulation, based on the harmonic approximation and continuum assumptions, cannot capture lattice discreteness or intrinsic anharmonic phonon–phonon scattering. Compared to wave-packet simulations that track wave propagation through MD trajectories,[47–49] FEM enables direct visualization of the spatial distribution of the steady-state wave field at specific frequencies, facilitating the observation of features such as interference fringes and localized hotspots. This method primarily provides qualitative visualization of wave localization phenomena, whereas molecular dynamics simulations naturally incorporate the aforementioned physical effects and enable quantitative analysis of thermal transport.

In summary, spectral thermal transport analysis establishes characteristic frequency ($\omega_c \approx 10$ THz) and length ($L_c \approx 100$ nm) scales for localization effects, with nonlinear deviations in the $1/\kappa$–$1/L$ relationship serving as a diagnostic indicator. The combined HNEMD–NEMD approach enables direct extraction of spectrally decomposed phonon MFPs without requiring Brillouin zone definitions, extending applicability to aperiodic structures. The thermal conductivity reduction in ap-GPnC originates primarily from low-frequency band flattening and systematic group velocity reduction induced by the breaking of translational symmetry. Dynamic transport simulations, eigenmode analysis, and elastic wave simulations characterize Anderson localization from the perspectives of macroscopic thermal conductivity length dependence, phonon mode-level localization signatures, and wave field visualization, respectively. The high Debye temperature and ultralong phonon MFPs of graphene amplify localization signatures, establishing GPnCs as an ideal platform for experimental verification.

See the supplementary material for details on the machine-learning molecular dynamics simulation, two-phonon model analysis, spectral heat current decomposition with in-plane/out-of-plane separation, lattice dynamics calculations, and elastic wave propagation simulations.

The authors acknowledge support from the Beijing Natural Science Foundation (Grant No. 3254051), the National Natural Science Foundation of China (Grant No. 12432013), and the China Postdoctoral Science Foundation (Grant No. 2023M741895). The calculations were performed on the "Explorer 1000" high-performance computing cluster at the High-Performance Computing Center of Tsinghua University.

AUTHOR DECLARATIONS

Conflict of Interest

The authors have no conflicts to disclose.

Author Contributions

Bin Liu: Formal analysis (equal); Investigation (equal); Writing – original draft (equal). **Zhiguo Tian:** Validation (equal); Writing – review & editing (equal). **Alexander A. Barinov:** Data curation (equal); Writing – review & editing (equal). **Moran Wang:** Conceptualization (equal); Supervision (equal); Writing – review & editing (equal).

DATA AVAILABILITY

The data that support the findings of this study are available within the article and its supplementary material.

REFERENCES

[1]T.-H. Liu, T. Wang, J. Zhou, X. Qian, and R. Yang, "Thermal-driven multi-carrier transport in electronic and energy materials," Appl. Phys. Rev. **12**, 031308 (2025).

[2]D. G. Cahill, S. K. Watson, and R. O. Pohl, "Lower limit to the thermal conductivity of disordered crystals," Phys. Rev. B **46**, 6131–6140 (1992).

[3]Y. Cheng, M. Nomura, S. Volz, and S. Xiong, "Phonon–dislocation interaction and its impact on thermal conductivity," J. Appl. Phys. **130**, 040902 (2021).

[4]Y. Guo and M. Wang, "Phonon hydrodynamics and its applications in nanoscale heat transport," Phys. Rep. **595**, 1–44 (2015).

[5]J. Hu, S. Schiffli, A. Vallabhaneni, X. Ruan, and Y. P. Chen, "Tuning the thermal conductivity of graphene nanoribbons by edge passivation and isotope engineering: A molecular dynamics study," Appl. Phys. Lett. **97**, 133107 (2010).

[6]B. Liu, V. I. Khvesyuk, A. A. Barinov, and M. Wang, "Effect of interfacial roughness on thermal boundary conductance: An elastic wave model using the Kirchhoff approximation," Int. J. Mech. Sci. **218**, 106993 (2022).

[7]R. Hu, S. Iwamoto, L. Feng, S. Ju, S. Hu, M. Ohnishi, N. Nagai, K. Hirakawa, and J. Shiomi, "Machine-learning-optimized aperiodic superlattice minimizes coherent phonon heat conduction," Phys. Rev. X **10**, 021050 (2020).

[8]T. Juntunen, O. Vänskä, and I. Tittonen, "Anderson localization quenches thermal transport in aperiodic superlattices," Phys. Rev. Lett. **122**, 105901 (2019).

[9]M. N. Luckyanova, J. Mendoza, H. Lu, B. Song, S. Huang, J. Zhou, M. Li, Y. Dong, H. Zhou, J. Garlow, L. Wu, B. J. Kirby, A. J. Grutter, A. A. Puretzky, Y. Zhu, M. S. Dresselhaus, A. Gossard, and G. Chen, "Phonon localization in heat conduction," Sci. Adv. **4**, eaat9460 (2018).

[10]Y. Ni and S. Volz, "Evidence of phonon Anderson localization on the thermal properties of disordered atomic systems," J. Appl. Phys. **130**, 190901 (2021).

[11]Y. Wang, C. Gu, and X. Ruan, "Optimization of the random multilayer structure to break the random-alloy limit of thermal conductivity," Appl. Phys. Lett. **106**, 073104 (2015).

[12]G. Chen, "Non-Fourier phonon heat conduction at the microscale and nanoscale," Nat. Rev. Phys. **3**, 555–569 (2021).

[13]Z. Zhang, Y. Guo, M. Bescond, J. Chen, M. Nomura, and S. Volz, "Coherent thermal transport in nano-phononic crystals: An overview," APL Mater. **9**, 081102 (2021).

[14]R. Hu and Z. Tian, "Direct observation of phonon Anderson localization in Si/Ge aperiodic superlattices," Phys. Rev. B **103**, 045304 (2021).

[15]P. Chakraborty, M. Nasiri, H. Cui, T. Maranets, and Y. Wang, "A comprehensive investigation of the two-phonon characteristics of heat conduction in superlattices," Crystals **15**, 654 (2025).

[16]J. Mendoza and G. Chen, "Anderson localization of thermal phonons leads to a thermal conductivity maximum," Nano Lett. **16**, 7616–7620 (2016).

[17]A. J. Gabourie, Z. Fan, T. Ala-Nissila, and E. Pop, "Spectral decomposition of thermal conductivity: Comparing velocity decomposition methods in homogeneous molecular dynamics simulations," Phys. Rev. B **103**, 205421 (2021).

[18]B. Liu, Y. Guo, V. I. Khvesyuk, A. A. Barinov, and M. Wang, "Heat conduction of multilayer nanostructures with consideration of coherent and incoherent phonon transport," Nano Res. **15**, 9492–9497 (2022).

[19]L. N. Maurer, S. Mei, and I. Knezevic, "Rayleigh waves, surface disorder, and phonon localization in nanostructures," Phys. Rev. B **94**, 045312 (2016).

[20]X. Wu, Z. Wu, T. Liang, Z. Fan, J. Xu, M. Nomura, and P. Ying, "Phonon coherence and minimum thermal conductivity in disordered superlattices," Phys. Rev. B **111**, 085413 (2025).

[21]N. Zen, T. A. Puurtinen, T. J. Isotalo, S. Chaudhuri, and I. J. Maasilta, "Engineering thermal conductance using a two-dimensional phononic crystal," Nat. Commun. **5**, 3435 (2014).

[22]S. Ju, S. Shimizu, and J. Shiomi, "Designing thermal functional materials by coupling thermal transport calculations and machine learning," J. Appl. Phys. **128**, 161102 (2020).

[23]K. Khot, B. Xiao, Z. Han, Z. Guo, Z. Xiong, and X. Ruan, "Phonon local non-equilibrium at Al/Si interface from machine learning molecular dynamics," J. Appl. Phys. **137**, 115301 (2025).

[24]B. Liu, Z. Tian, A. A. Barinov, and M. Wang, "Enhanced heat conduction in diamond/copper composites via interconnected structures: Machine learning molecular dynamics simulation," Int. J. Therm. Sci. **221**, 110501 (2026).

[25]H. Liu, X. Qian, H. Bao, C. Y. Zhao, and X. Gu, "High-temperature phonon transport properties of SnSe from machine-learning interatomic potential," J. Phys.: Condens. Matter **33**, 405401 (2021).

[26]K. Xu, H. Bu, S. Pan, E. Lindgren, Y. Wu, Y. Wang, J. Liu, K. Song, B. Xu, Y. Li, T. Hainer, L. Svensson, J. Wiktor, R. Zhao, H. Huang, C. Qian, S. Zhang, Z. Zeng, B. Zhang, B. Tang, Y. Xiao, Z. Yan, J. Shi, Z. Liang, J. Wang, T. Liang, S. Cao, Y. Wang, P. Ying, N. Xu, C. Chen, Y. Zhang, Z. Chen, X. Wu, W. Jiang, E. Berger, Y. Li, S. Chen, A. J. Gabourie, H. Dong, S. Xiong, N. Wei, Y. Chen, J. Xu, F. Ding, Z. Sun, T. Ala-Nissila, A. Harju, J. Zheng, P. Guan, P. Erhart, J. Sun, W. Ouyang, Y. Su, and Z. Fan, "GPUMD 4.0: A high-performance molecular dynamics package for versatile materials simulations with machine-learned potentials," Mater. Genome Eng. Adv. **3**, e70028 (2025).

[27]M. Sledzinska, B. Graczykowski, J. Maire, E. Chavez-Angel, C. M. Sotomayor-Torres, and F. Alzina, "2D phononic crystals: Progress and prospects in hypersound and thermal transport engineering," Adv. Funct. Mater. **30**, 1904434 (2020).

[28]T. Vasileiadis, J. Varghese, V. Babacic, J. Gomis-Bresco, D. Navarro Urrios, and B. Graczykowski, "Progress and perspectives on phononic crystals," J. Appl. Phys. **129**, 160901 (2021).

[29]Z. Fan, Y. Xiao, Y. Wang, P. Ying, S. Chen, and H. Dong, "Combining linear-scaling quantum transport and machine-learning molecular dynamics to study thermal and electronic transports in complex materials," J. Phys.: Condens. Matter **36**, 245901 (2024).

[30]M. M. Sadeghi, I. Jo, and L. Shi, "Phonon-interface scattering in multilayer graphene on an amorphous support," Proc. Natl. Acad. Sci. U. S. A. **110**, 16321–16326 (2013).

[31]H. Zhang, C. Hua, D. Ding, and A. J. Minnich, "Length dependent thermal conductivity measurements yield phonon mean free path spectra in nanostructures," Sci. Rep. **5**, 9121 (2015).

[32]Z. Fan, Z. Zeng, C. Zhang, Y. Wang, K. Song, H. Dong, Y. Chen, and T. Ala-Nissila, "Neuroevolution machine learning potentials: Combining high accuracy and low cost in atomistic simulations and application to heat transport," Phys. Rev. B **104**, 104309 (2021).

[33]X. Zhou, Y. Liu, B. Tang, J. Wang, H. Dong, X. Xiu, S. Chen, and Z. Fan, "Million-atom heat transport simulations of polycrystalline graphene approaching first-principles accuracy enabled by neuroevolution potential on desktop GPUs," J. Appl. Phys. **137**, 014305 (2025).

[34]P. Rowe, V. L. Deringer, P. Gasparotto, G. Csányi, and A. Michaelides, "An accurate and transferable machine learning potential for carbon," J. Chem. Phys. **153**, 034702 (2020).

[35]Y. Xiao, Y. Liu, Z. Tan, B. Zhang, K. Xu, Z. Fan, S. Chen, S. Xiong, and H. Dong, "Optimizing thermoelectric performance of graphene antidot lattices via quantum transport and machine-learning molecular dynamics simulations," Phys. Rev. Mater. **9**, 084603 (2025).

[36]Z. Fan, Y. Wang, P. Ying, K. Song, J. Wang, Y. Wang, Z. Zeng, K. Xu, E. Lindgren, J. M. Rahm, A. J. Gabourie, J. Liu, H. Dong, J. Wu, Y. Chen, Z. Zhong, J. Sun, P. Erhart, Y. Su, and T. Ala-Nissila, "GPUMD: A package for

constructing accurate machine-learned potentials and performing highly efficient atomistic simulations," J. Chem. Phys. **157**, 114801 (2022).
[37]Y. Wang, Z. Fan, P. Qian, M. A. Caro, and T. Ala-Nissila, "Quantum-corrected thickness-dependent thermal conductivity in amorphous silicon predicted by machine learning molecular dynamics simulations," Phys. Rev. B **107**, 054303 (2023).
[38]Y. Wang, Z. Fan, P. Qian, M. A. Caro, and T. Ala-Nissila, "Density dependence of thermal conductivity in nanoporous and amorphous carbon with machine-learned molecular dynamics," Phys. Rev. B **111**, 094205 (2025).
[39]S. Hu, Z. Zhang, P. Jiang, J. Chen, S. Volz, M. Nomura, and B. Li, "Randomness-induced phonon localization in graphene heat conduction," J. Phys. Chem. Lett. **9**, 3959–3968 (2018).
[40]Y. Wang, H. Huang, and X. Ruan, "Decomposition of coherent and incoherent phonon conduction in superlattices and random multilayers," Phys. Rev. B **90**, 165406 (2014).
[41]Z. Fan, H. Dong, A. Harju, and T. Ala-Nissila, "Homogeneous nonequilibrium molecular dynamics method for heat transport and spectral decomposition with many-body potentials," Phys. Rev. B **99**, 064308 (2019).
[42]B. Liu, Z. Tian, A. A. Barinov, and M. Wang, "Interfacial and coherent thermal transport of phonons in Bi_2Te_3/Sb_2Te_3 superlattices," Int. J. Heat Mass Transfer **258**, 128283 (2026).
[43]E. Lindgren, M. Rahm, E. Fransson, F. Eriksson, N. Österbacka, Z. Fan, and P. Erhart, "calorine: A Python package for constructing and sampling neuroevolution potential models," J. Open Source Software **9**, 6264 (2024).
[44]A. Togo, L. Chaput, T. Tadano, and I. Tanaka, "Implementation strategies in phonopy and phono3py," J. Phys.: Condens. Matter **35**, 353001 (2023).
[45]X. Wu, Y. Cheng, S. Huang, and S. Xiong, "Phonon resonance effect and defect scattering in covalently bonded carbon nanotube networks," Phys. Rev. Appl. **22**, 024038 (2024).
[46]S. Xiong, K. Sääskilahti, Y. A. Kosevich, H. Han, D. Donadio, and S. Volz, "Blocking phonon transport by structural resonances in alloy-based nanophononic metamaterials leads to ultralow thermal conductivity," Phys. Rev. Lett. **117**, 025503 (2016).
[47]T. Maranets and Y. Wang, "How phonon coherence develops and contributes to heat conduction in periodic and aperiodic superlattices," Int. J. Therm. Sci. **217**, 110018 (2025).
[48]C. Shao, Q. Rong, M. Hu, and H. Bao, "Probing phonon–surface interaction by wave-packet simulation: Effect of roughness and morphology," J. Appl. Phys. **122**, 155104 (2017).
[49]C. Shao, Q. Rong, N. Li, and H. Bao, "Understanding the mechanism of diffuse phonon scattering at disordered surfaces by atomistic wave-packet investigation," Phys. Rev. B **98**, 155418 (2018).